5610–5624 *Nucleic Acids Research, 2007, Vol. 35, No. 16* *Published online 17 August 2007*
doi:10.1093/nar/gkm606

Identification of determinants in the protein partners aCBF5 and aNOP10 necessary for the tRNA:Ψ55-synthase and RNA-guided RNA:Ψ-synthase activities

Sébastien Muller, Jean-Baptiste Fourmann, Christine Loegler, Bruno Charpentier* and Christiane Branlant

Laboratoire de Maturation des ARN et Enzymologie Moléculaire, UMR 7567 CNRS-UHP, Nancy Université, Université Henri Poincaré-BP 239, 54506 Vandoeuvre-Lès-Nancy cedex, France

Received July 3, 2007; Revised and Accepted July 25, 2007

ABSTRACT

Protein aNOP10 has an essential scaffolding function in H/ACA sRNPs and its interaction with the pseudouridine(Ψ)-synthase aCBF5 is required for the RNA-guided RNA:Ψ-synthase activity. Recently, aCBF5 was shown to catalyze the isomerization of U55 in tRNAs without the help of a guide sRNA. Here we show that the stable anchoring of aCBF5 to tRNAs relies on its PUA domain and the tRNA CCA sequence. Nonetheless, interaction of aNOP10 with aCBF5 can counterbalance the absence of the PUA domain or the CCA sequence and more generally helps the aCBF5 tRNA:Ψ55-synthase activity. Whereas substitution of the aNOP10 residue Y14 by an alanine disturbs this activity, it only impairs mildly the RNA-guided activity. The opposite effect was observed for the aNOP10 variant H31A. Substitution K53A or R202A in aCBF5 impairs both the tRNA:Ψ55-synthase and the RNA-guided RNA:Ψ-synthase activities. Remarkably, the presence of aNOP10 compensates for the negative effect of these substitutions on the tRNA: Ψ55-synthase activity. Substitution of the aCBF5 conserved residue H77 that is expected to extrude the targeted U residue in tRNA strongly affects the efficiency of U55 modification but has no major effect on the RNA-guided activity. This negative effect can also be compensated by the presence of aNOP10.

INTRODUCTION

Isomerization of uridine into pseudouridine (5-ribosyluracil, Ψ) is a prevalent post-transcriptional modification of cellular RNAs (1) and this modified residue is frequently found in functionally important RNA regions. Consistently, an important role of Ψ residues was demonstrated for specific codon–anticodon recognition and ribosome function (2–8). Furthermore, one of the highly conserved Ψ residue in U2 snRNA was found to play a key role in pre-mRNA splicing (9,10).

Two types of catalysts can generate Ψ residues at specific sites in a pre-existing polyribonucleotide chains. One type consists in a single protein with an RNA:Ψ-synthase activity. It recognizes specifically one or more RNA segments or motifs and converts the targeted U residues within these segments into Ψ residues. A large panel of such RNA:Ψ-synthases are found in most cell types and they are up to now the unique system detected in bacteria (11). These bacterial RNA:Ψ-synthases were the first to be characterized (12–15). The search for their homologs by inspection of various genomes led to the classification of these enzymes into five families, TruA, TruB, TruD, RsuA, RluA (16–18). Based on sequence alignment and 3D structure analysis of the catalytic domains of several RNA:Ψ-synthases, five conserved structural motifs (I, II, IIa, III and IIIa) were identified and they represent the signature for RNA:Ψ-synthases activity (16,19,20). Although only a limited number of amino acids in these motifs are conserved, these motifs have highly conserved conformations in the 3D structures established for RNA:Ψ-synthases (11). The few conserved amino acids play important roles for catalysis: a universally conserved aspartate residue in motif II is the essential catalytic amino acid (17,21–24). A conserved basic residue (Arg or Lys) in motif III makes a salt bridge with the catalytic Asp residue. A conserved Tyr residue in motif IIa has a stacking interaction with the uracyl residue to be modified in the target RNA (25). Two other

*To whom correspondence should be addressed. Tel: 33 3 83 68 43 16; Fax: 33 3 83 68 43 07; Email: bruno.charpentier@maem.uhp-nancy.fr

The authors wish it to be known that, in their opinion, the first two authors should be regarded as joint First Authors.

hydrophobic residues, a leucine in motif IIIa and an isoleucine or a valine residue in motif III, are also highly conserved, but their functional implication in the catalytic mechanism is less understood (19,25).

In the various RNA:Ψ-synthases identified up to now, the conserved catalytic domain is associated with a large variety of additional domains, which are likely involved in the specific recognition of the target RNA motif. One of these domains, the PUA domain (PseudoUridine and Archaeosine tRNA guanine transglycosylase), has largely been studied. It is found at the C-terminus of members of the TruB family of RNA:Ψ-synthases (25–30). As deduced from the crystal structure of the complex formed between the *Escherichia coli* TruB enzyme and the T stem-loop structure of tRNA (31), the PUA domain is expected to play a key role in RNA recognition by interacting with the CCA 3′-terminal sequence of tRNAs (25). This proposed interaction of TruB with a sequence common to all tRNAs fits with the general activity of TruB at position 55 of all elongator tRNAs.

The second type of catalyst for U to Ψ conversion consists in RNP complexes containing a small RNA with H/ACA motifs (the H/ACA snoRNAs and scaRNAs in Eukarya and H/ACA sRNAs in archaea) and a well-defined set of proteins (32–34). One of these proteins denoted aCBF5 in archaea, Cbf5p in yeast and CBF5/NAP57/Dyskerin in human displays the characteristic motifs I, II, IIa, III and IIIa found in RNA:Ψ-synthases and belongs to the TruB family of RNA:Ψ-synthase (16,19). In each RNP, the RNA component base pairs with one or more targeted RNA sequences and through this interaction acts as a guide to specify the uridyl residues that will be modified (32–34). Knowledge on the mechanism of the H/ACA RNPs activity is largely based on data obtained with the archaeal H/ACA RNPs that could be reconstituted using an *in vitro* transcribed RNA and recombinant proteins (35,36). In addition to the protein bearing the signature of RNA:Ψ-synthases, each H/ACA RNP contains three distinct proteins (NOP10, GAR1 and NHP2 in human; Nop10p, Gar1p and Nhp2p in yeast; and aNOP10, aGAR1 and L7Ae in archaea). The three archaeal aCBF5, aNOP10 and aGAR1 proteins form an heterotrimer in solution (35,36). The 3D structures of the aCBF5-aNOP10 heterodimer and aCBF5-aNOP10-aGAR1 heterotrimer complexes were solved by X-ray crystallography (27–29).

Very recently, the crystal structure of an entire archaeal box H/ACA sRNP was determined (30). Through reconstitution experiments, we showed that in archaea the aCBF5–aNOP10 complex is the minimal set of proteins required to get an RNA-guided RNA:Ψ-synthase activity (36). However, the two other proteins aGAR1 and L7Ae both increase the efficiency of the catalytic reaction. Formation of an H/ACA sRNA–aCBF5–aNOP10 complex depends upon aCBF5 association with the sRNA and the conserved ACA motif in the sRNA plays an essential role for this association (35,36). More precisely, the PUA domain of aCBF5 interacts with the ACA motif of H/ACA sRNAs (27,30). According to our previous reconstitution assays, formation of an sRNA–aCBF5–aNOP10 complex is required for binding of the RNA substrate and recent structural studies on NOP10 revealed its capability to bind RNA (37). By *in vitro* reconstitution of H/ACA sRNPs with truncated aNOP10 proteins, we showed that its C-terminal half is sufficient for sRNP activity, whereas its N-terminal half reinforces the aCBF5-aNOP10 interaction (27). The L7Ae protein binds a K-turn motif present in each stem-loop structures of the archaeal H/ACA sRNAs (35,36,38,39). The direct interaction of L7Ae with aNOP10 and the sRNA stabilizes the association of the other proteins with the sRNA (30). In light of the higher rate of pseudouridylation observed in the presence of aGAR1, we proposed that protein aGAR1 might enhance the turnover of the reaction catalyzed by the sRNP (36).

A recent *in vitro* study showed that in addition to its central role in the RNA guided activity of H/ACA sRNPs, the archaeal aCBF5 enzyme has the ability to convert residue U55 of an *in vitro* transcribed tRNA into a Ψ residue (40). This activity seems to be increased in the presence of the L7Ae, aNOP10 and aGAR1 set of proteins (40). Altogether, these data revealed the ability of aCBF5 to act without guide RNA in case of a tRNA substrate. However, an *in vivo* dual role of aCBF5, as rRNA:Ψ-synthase when included in H/ACA sRNPs and as tRNA:Ψ55-synthase when acting as a free protein, is still not demonstrated since another archaeal RNA:Ψ-synthase PusX/Pus10 is also able to catalyze U to Ψ conversion at position 55 in tRNAs. Nevertheless, the capability of aCBF5 to act as a free protein and in sRNPs represented an opportunity: (i) to delineate the tRNA structures needed to get an activity of aCBF5 in the absence of guide RNA, (ii) to compare the aNOP10 and aGAR1 requirements for the guided and non guided activity of aCBF5, (iii) to compare the aCBF5 amino acid requirement for its guided and non-guided activity. Here, by site-directed mutagenesis of the *Pyrococcus abyssi* and *Saccharomyces cerevisiae* tRNAs, we show that a truncated version of tRNA including the acceptor and TΨC stem-loop structures linked by a flexible sequence is sufficient to get aCBF5 activity in the absence of a guide RNA. In the absence of the 3′ terminal CCA, the aCBF5 activity becomes strictly dependent on either aNOP10 or aGAR1. Furthermore, by site-directed mutagenesis of both aNOP10 and aCBF5 we demonstrate distinct amino acid requirements for the RNA-guided and non RNA-guided activities of aCBF5. The results obtained are discussed based on the 3D structures of the archaeal H/ACA sRNP proteins and their complexes.

MATERIALS AND METHODS

Production of protein variants

The aCBF5 D82A and CΔ(PUA) protein variants carrying, respectively, an Asp to Ala substitution at position 82 and a truncation of the PUA domain, were previously described (27,36). The PCR approach was used for site-directed mutagenesis of protein aCBF5 (K53A, H77A and R202A variants) and aNOP10 (Y14A, H31A and P32A variants). The sequence of the oligonucleotides used for the PCR reactions are available upon request.

Purification of recombinant proteins

Wild-type and variant aCBF5 and aNOP10 proteins as well as the aGAR1 and TruB proteins were produced as GST fusion proteins as previously described (36). The GST moiety was removed by cleavage with the PreScission protease. The various proteins were stored at −80°C in the following buffer 150 mM NaCl, 1 mM EDTA, 1 mM DTT, glycerol 10%, 50 mM Tris–HCl pH 7.

In vitro transcription of tRNAs, H/ACA sRNA and the sRNP target RNA

Wild-type and mutated tRNA transcripts, the Pab91 H/ACA sRNA and the RNA target RNA-S (36) were produced by *in vitro* transcription of PCR products. The forward primers used for PCR amplification generated the T7 RNA polymerase promoter. DNA templates for amplifications of sequences coding for the WT yeast $tRNA^{Asp}$ and variants of this tRNA (ΔT-$tRNA^{Asp}$, ΔD-$tRNA^{Asp}$,) were a generous gift of C. Florentz (IBMC, Strasbourg). Additional yeast $tRNA^{Asp}$ variants (Δa.c.-$tRNA^{Asp}$, Δacceptor-$tRNA^{Asp}$, Δacceptor-$tRNA^{Asp}$-U55C) were produced by site-directed mutagenesis in the course of the PCR amplification. The sequence coding for the WT *P. abyssi* $tRNA^{Asp}$ was PCR amplified using genomic DNA from the *P. abyssi* GE5 strain. Sequences encoding the variants $tRNA^{Asp}$-ACA and $tRNA^{Asp}$-ΔCCA were obtained by using a reverse primer carrying the mutated sequence. Sequences encoding the WT semi-$tRNA^{Asp}$ or the variant semi-$tRNA^{Asp}$-ΔCCA or semi-$tRNA^{Asp}$-U55C were obtained by hybridization of two complementary oligonucleotides. The other archaeal $tRNA^{Asp}$ variants ($tRNA^{Asp}$-U55C) were produced by site-directed mutagenesis in the course of a PCR amplification. DNA templates for production of the *P. abyssi* Pab91 sRNA and its target RNA (RNA-S) were previously described (36). The RNA transcripts were purified by denaturing gel electrophoresis. Labeling was done at their 5′ end for EMSA experiments or during *in vitro* transcription by incorporation of [α-^{32}P]CTP for the pseudouridylation assays. Conditions for transcription and labeling were previously described (41).

Electrophoresis mobility shift assays (EMSA)

EMSA were performed in the conditions previously described (36,41). Briefly, radiolabeled RNAs (50 fmol) were incubated in buffer D [150 mM KCl, 1.5 mM $MgCl_2$, 0.2 mM EDTA and 20 mM HEPES (pH 7.9)] with proteins at a 200 nM concentration, at 65°C for 10 min. To test for the association of the Pab91 sRNP with its target RNA (complex CII), 2.5 pmol of RNA-S were added. Complexes were visualized by autoradiography after fractionation by non-denaturing polyacrylamide gel electrophoresis.

In vitro pseudouridylation assay

The tRNA:Ψ55-synthase activities of purified aCBF5 or H/ACA–RNP complexes were measured by the nearest-neighbor approach in the conditions previously described (36,41). The RNA-guided activity of reconstituted H/ACA sRNPs was measured as previously described by mixing ∼4 pmol of Pab91 sRNA with ∼150 fmol of the [α-^{32}P]CTP-labeled target RNA-S (36). The non-RNA-guided reaction of aCBF5 on tRNA was tested on ∼50 fmol of [α-^{32}P]CTP-labeled tRNAs. For both RNA-guided and non-RNA-guided reactions, samples were pre-incubated at 65°C and the reaction was started by addition of the proteins (200 nM each). Aliquots were collected at different time points, the RNAs were extracted and then digested by RNase T2. The resulting 3′-mononucleotides were fractionated by thin-layer cellulose chromatography. The radioactivity in the spots was quantified using the ImageQuant software after exposure of a phosphorimager screen. The amount of Ψ residue formed was determined taking into account the total number of U residues in the tRNA or RNA-S molecules. Some of the values given in the text are expressed with standard errors of the mean values. All the time-course analyses were repeated at least three times and gave reproducible data. Some control experiments were performed with the *E. coli* TruB recombinant protein. The same procedure was used to measure the activity, except that the reaction was performed at 37°C.

Mapping the site of pseudouridylation in tRNAs

We used the *N*-cyclohexyl-*N*′-(2-morpholinoethyl)-carbodiimide metho-*p*-toluolsulfonate (CMCT) modification protocol of (42), adapted by (43). CMCT modifications were performed with 0.5 μg of *in vitro* transcribed archaeal or yeast $tRNA^{Asp}$. Positions of CMCT modifications were identified by primer extension analysis, using the AMV RT (QBiogene, USA) in the conditions previously described (44) and the primer oligonucleotides OG4891 for archaeal $tRNA^{Asp}$ and OG5302 for *S. cerevisiae* $tRNA^{Asp}$ (Figure 1A1 and B1). Primers were 5′-end labeled using [γ-^{32}P]ATP (3000 Ci/mmol) and T4 polynucleotide kinase. RNA sequencing was done with 4 μg of *in vitro* transcribed RNA [for details on the technique, see (45)].

RESULTS

The kinetics of U to Ψ conversion at position 55 in tRNAs is enhanced in the presence of proteins aNOP10 and aGAR1

Previous studies revealed a U to Ψ conversion activity of the *P. furiosus* aCBF5 protein at position 55 in the *P. furiosus* $tRNA^{Asp}$(GUC), i.e. a tRNA:Ψ55-synthase activity. Such an activity is enhanced in the presence of the aNOP10, aGAR1 and L7Ae proteins set (40). For a deeper understanding of these activation properties, here we quantified the relative stimulation effects of proteins aNOP10, aGAR1 and L7Ae alone and in various combinations, on the tRNA:Ψ55-synthase activity of aCBF5. The assays were performed with the *P. abyssi* recombinant proteins aCBF5, aNOP10, aGAR1 and L7Ae, and with both *P. abyssi* $tRNA^{Asp}$(GUC) and *S. cerevisiae* $tRNA^{Asp}$(GUC) substrates (Figure 1A1 and B1). We used the nearest neighbor and the RT–CMCT approaches in order to verify that modifications occurred only at position 55 in tRNAs. For the

nearest-neighbor approach, both substrates were labeled by incorporation of [α-^{32}P]CTP during transcription. After the pseudouridylation reactions, the tRNA transcripts were digested with RNase T2 and the products were fractionated by 2D chromatography (Figure 1A2 and B2). CMCT modifications followed by alkaline treatments were performed on cold RNA transcripts, and positions of modifications were identified by reverse transcription (Figure 1A3 and B3) using oligonucleotide primers that were complementary to the 3′ terminal sequence of tRNAs (Figure 1A1 and B1). The pseudouridylation reaction was performed at 65°C, for 80 min using a 200 nM concentration of each protein. Time point experiments were performed on the *P. abyssi* tRNA^{Asp} with: (i) aCBF5 alone, (ii) aCBF5 in the presence of aNOP10 or aGAR1, or of both proteins and (iii) aCBF5 in the presence of aNOP10 and L7Ae, or the three L7Ae, aNOP10, aGAR1 proteins. Aliquots of the reaction mixtures were analyzed after 5, 10, 20, 40 and 80 min of incubation (Figures 1A4 and S1). For comparison, a time point experiment was performed at 37°C with a recombinant *E. coli* TruB enzyme (Figure 1A2).

Altogether, the results obtained demonstrated that protein aCBF5 is able to modify the *P. abyssi* and *S. cerevisiae* tRNA^{Asp} at the same high level after 80 min of incubation (~0.85 mol ± 0.05 and ~0.9 mol ± 0.05 of Ψ per mol of tRNA, respectively). In both cases, only a slight increase of the level of modification was observed in the presence of aNOP10 and aGAR1 (Figure 1A2 and B2). However, as evidenced by the time point experiments, although the kinetics of the reaction with aCBF5 at 65°C is very fast compared to that for TruB at 37°C, it was markedly increased in the presence of aNOP10 or aGAR1. On the contrary, protein L7Ae showed no stimulatory effect (see Supplementary Data, Figure S1), which is in contrast to data obtained for the sRNA-guided activity of aCBF5 (35,36). The CMCT analysis did confirm that aCBF5 acted only at position 55 in both tRNAs. Finally, we confirmed the general capability of aCBF5 to act at position 55 in tRNAs by using other archaeal and bacterial transcripts as the substrates (data not shown).

Altogether, we concluded that aCBF5 has the ability to modify various tRNAs at position 55 and this independently of the organisms from which they originate. The reaction is very rapid and is nearly complete after a 15-min incubation. However, the kinetics of this reaction is markedly increased in the presence of aNOP10 or aGAR1. In this case, the reaction is completed after a 7-min incubation. Furthermore, the catalytic property of aCBF5, alone or acting in the presence of aNOP10 and aGAR1 is highly specific of position 55.

Proteins aNOP10 and aGAR1 have a strong stimulatory effect on Ψ55 formation in the absence of the aCBF5 PUA domain or of the tRNA 3′ terminal CCA motif

Our previous data on the sRNA guided activity of aCBF5 revealed a strong importance of the PUA domain of aCBF5 for this activity and a negative effect of mutations in the ACA sequence of the H/ACA sRNA (27). The recent crystal structure of an H/ACA sRNP demonstrated a direct contact of the PUA domain with the ACA motif (30). Therefore, we tested whether the PUA domain was also required for the activity of aCBF5 at position 55 in tRNAs. As shown in Figure 2, no U to Ψ conversion occurred in the *P. abyssi* tRNA^{Asp} when it was incubated with an aCBF5 protein lacking the PUA domain (CΔ(PUA)). Interestingly, this tRNA:Ψ55-synthase activity was partially restored in the presence of the aNOP10 and aGAR1 proteins pair (CΔ(PUA)NG). However, the kinetics was slower and the efficiency of modification after 80 min was lower. The individual aNOP10 and aGAR1 proteins had similar but very low capabilities to restore the tRNA:Ψ55-synthase activity of the truncated aCBF5 protein (Figure 2).

As previous data had revealed the absence of aCBF5 activity on a tRNA lacking the 3′ terminal CCA motif (40), we tested whether aNOP10 or aGAR1 or both proteins can compensate for the absence of this motif (Figure 3). We found in this case that individual aNOP10 or aGAR1 can restore a strong aCBF5 activity (CN and CG, respectively) at position 55 of tRNAs and this activity was reinforced to some extent when the two proteins were present (CNG). Remarkably, modification with the CNG complex was almost complete after a 10-min incubation, even in the absence of the CCA motif (Figure 3). The truncated tRNA was modified at a slower rate and lower yield, when TruB was used as the catalyst. Taken together, the data revealed a very important role of the PUA domain for the aCBF5 tRNA:Ψ55-synthase activity and showed the capability of the aNOP10–aGAR1 protein pair to compensate partially for its absence. Moreover, the presence of the auxiliary proteins fully restores the aCBF5 activity in the absence of the tRNA CCA 3′ terminal motif.

The aNOP10–aGAR1 protein pair can compensate for severe truncations in tRNAs

As we found that aNOP10 and aGAR1 can compensate for CCA deletion, we wondered whether they can compensate for more severe truncations in tRNAs. As aCBF5 was acting on the *S. cerevisiae* tRNA^{Asp}, and as several variants of this tRNA had already been produced (Figure 4A1), we tested the capability of aCBF5 (C) and the aCBF5–aNOP10–aGAR1 complex (CNG) to convert U55 into a Ψ residue in these truncated tRNAs (Figure 4A2). In RNAs ΔT-tRNA^{Asp}, Δa.c.-tRNA^{Asp} and ΔD-tRNA^{Asp}, the T stem-loop, the anticodon stem-loop, and the D stem-loop were deleted, respectively. The acceptor stem was truncated in RNA Δacceptor-tRNA^{Asp}, but the CCA 3′-terminal motif was conserved (Figure 4A1). Obviously, no Ψ formation was detected in the ΔT-tRNA^{Asp} substrate which was lacking residue U55. Only a very low level of modification was detected in the Δa.c.-tRNA^{Asp} when aCBF5 was used alone, while a high level of modification was detected when aNOP10 and aGAR1 were present in the incubation mixture (Figure 4A2). Similarly, no modification of the Δacceptor-tRNA^{Asp} substrate was observed when the incubation was performed with aCBF5 alone, whereas almost a complete modification was detected for these two

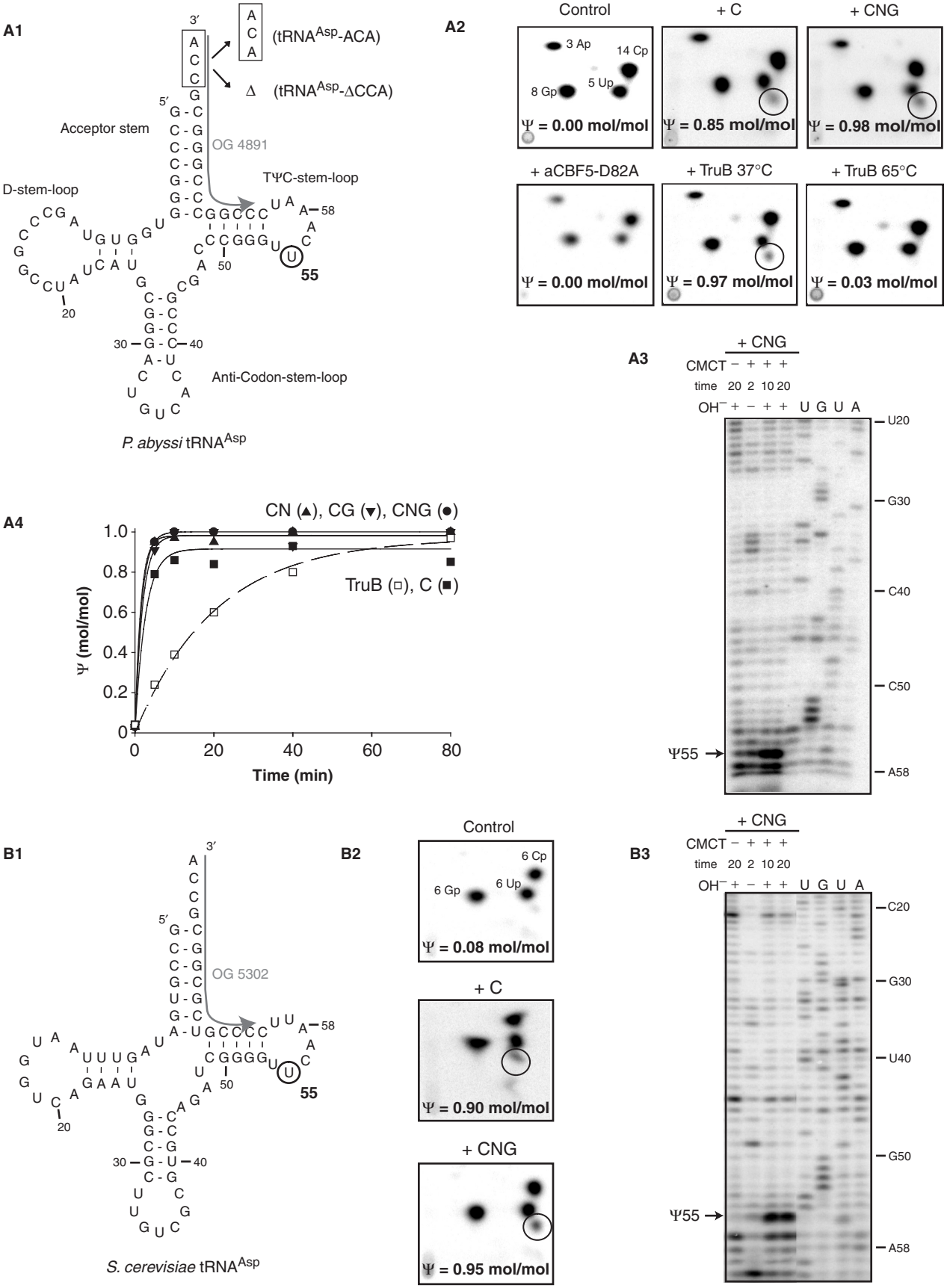
A1
(tRNA^Asp-ACA)
Δ (tRNA^Asp-ΔCCA)
Acceptor stem
OG 4891
TΨC-stem-loop
D-stem-loop
Anti-Codon-stem-loop
P. abyssi tRNA^Asp
A2
Control
+ C
+ CNG
3 Ap
14 Cp
8 Gp
5 Up
Ψ = 0.00 mol/mol
Ψ = 0.85 mol/mol
Ψ = 0.98 mol/mol
+ aCBF5-D82A
+ TruB 37°C
+ TruB 65°C
Ψ = 0.00 mol/mol
Ψ = 0.97 mol/mol
Ψ = 0.03 mol/mol
A3
+ CNG
CMCT
time 20 2 10 20
OH⁻
U G U A
Ψ55
A4
CN (▲), CG (▼), CNG (●)
TruB (□), C (■)
Ψ (mol/mol)
Time (min)
B1
OG 5302
S. cerevisiae tRNA^Asp
B2
Control
6 Cp
6 Gp
6 Up
Ψ = 0.08 mol/mol
+ C
Ψ = 0.90 mol/mol
+ CNG
Ψ = 0.95 mol/mol
B3
+ CNG
CMCT
time 20 2 10 20
OH⁻
U G U A
Ψ55

truncated tRNAs in the presence of aNOP10 and aGAR1 (Figure 4A2). Modification only occurred at position 55 in the truncated substrates since it disappeared after U to C mutation at this position (Δacceptor-tRNA^{Asp}-U55C).

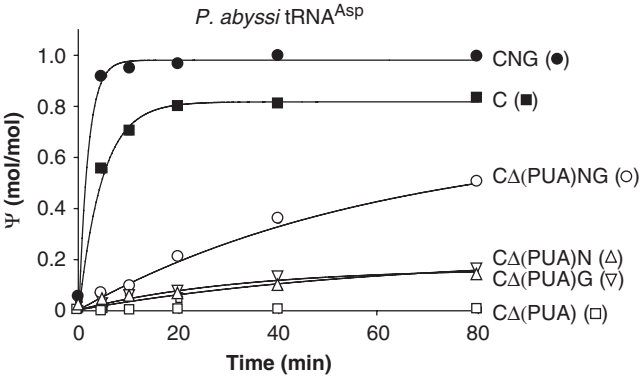

Figure 2. The PUA domain of aCBF5 is required for Ψ55 formation. Time-course experiments of Ψ55 formation were performed as in Figure 1 panel A4, using either the full-length aCBF5 (C) or aCBF5 truncated of its PUA domain [CΔ(PUA)], in the presence or the absence of the aNOP10 and/or aGAR1 proteins [CNG, CΔ(PUA)N, CΔ(PUA)G and CΔ(PUA)NG].

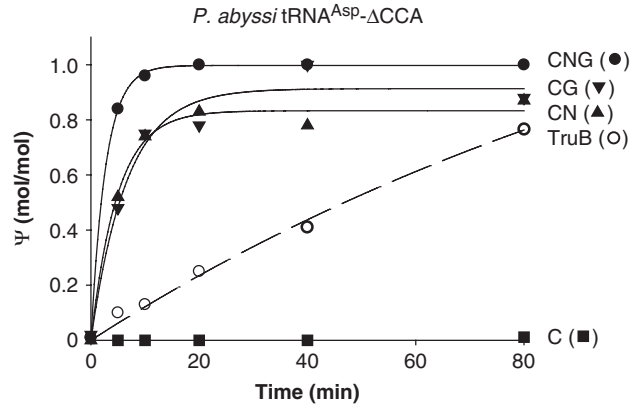

Figure 3. The aCBF5–aNOP10–aGAR1 complex can efficiently modify a tRNA lacking a 3′ CCA sequence. Time-course experiments of Ψ55 formation in the variant tRNA^{Asp}-ΔCCA by the *E. coli* TruB enzyme or various combinations of the aCBF5 (C), aNOP10 (N) and aGAR1 (G) proteins (same conditions as in Figure 2).

Interestingly, the ΔD-tRNA^{Asp} was modified by aCBF5 at a high level in absence of the auxiliary proteins (Figure 4A2). As expected from previous data (46), TruB was able to modify a tRNA lacking the acceptor stem without the need for auxiliary proteins. Based on the activity of aCBF5 alone on the ΔD-tRNA^{Asp}, we concluded that aCBF5 alone, like TruB, does not need the tRNA 3D structure for activity. However, in contrast to TruB, to act alone aCBF5 needs the presence of its target T stem-loop but also the anticodon stem-loop and the acceptor stem.

Roovers *et al.* (40) had found that aCBF5 does not modify a truncated *P. furiosus* tRNA^{Asp} that contains the acceptor stem fused to the T stem-loop. We confirmed that for an equivalent *P. abyssi* substrate, no activity was restored upon addition of the aNOP10–aGAR1 protein pair (data not shown). However, as aCBF5 was active on the yeast ΔD-tRNA^{Asp} substrate, we postulated that flexibility between the acceptor stem and the T stem-loop might be an important feature for aCBF5 activity. Therefore, we produced a truncated RNA substrate (semi-tRNA^{Asp}) by truncation of the *P. abyssi* tRNA^{Asp}, which contained a UGAC single-stranded sequence acting as a flexible link between the acceptor stem and the T stem-loop (Figure 4B1). The aCBF5 protein alone had a modest but significant activity on this substrate (mean value $<0.2\,mol.mol^{-1}$). This activity was abolished in the absence of the 3′ terminal CCA sequence (Figure 4B2). However, in the presence of the aNOP10–aGAR1 protein pair both the semi-tRNA^{Asp} and semi-tRNA^{Asp}-ΔCCA lacking the 3′ terminal CCA sequence were almost completely modified. As expected, TruB was active on both substrates in the absence of auxiliary proteins. Hence, we concluded that the aCBF5–aNOP10–aGAR1 heterotrimer, but not aCBF5 alone, has catalytic properties similar to that of TruB.

aNOP10 reinforces the formation of aCBF5–tRNA complexes

As the aNOP10 stimulatory effect on the aCBF5 activity seemed to consist in an increase of the kinetics of the reaction (36), and as aNOP10 was known to bind RNA (30,37), we hypothesized that aNOP10 might facilitate the association of aCBF5 with the tRNA substrate. To test

Figure 1. The *P. abyssi* aCBF5 protein modifies position 55 in *P. abyssi* and *S. cerevisiae* tRNA^{Asp}. (**A1**) Secondary structure of the *P. abyssi* tRNA^{Asp} used in this study. Residue U55 is circled. The CCA sequence at the 3′ end is boxed. The CCA to ACA substitution and the CCA deletion in variants tRNA^{Asp}-ACA and tRNA^{Asp}-ΔCCA, are shown. (**A2**) 2D Thin-layer-chromatography (TLC) analysis of Ψ formation in *P. abyssi* tRNA^{Asp}. The *P. abyssi* tRNA^{Asp} transcript was labeled by the incorporation of [α-^{32}PCTP] during transcription. The ^{32}P-labeled tRNA substrate (50 fmol) was mixed with either the *P. abyssi* aCBF5 protein (C), or its aCBF5-D82A variant, or the aCBF5-aNOP10–aGAR1 complex (CNG), or the *E. coli* TruB enzyme (200 nM each). Incubation was performed for 80 min at 65°C for the archaeal enzymes and at 37 or 65°C for TruB. After T2 RNase digestion, the amount of Ψ residue formed was measured by 2D TLC and expressed in moles per moles of tRNA. The data shown are representative examples of at least three independent experiments. (**A3**) CMC/RT analysis for the detection of Ψ formation at position 55 in the *P. abyssi* tRNA^{Asp}. The unlabeled tRNA (2 μg, 80 pmol) was incubated with proteins aCBF5, aNOP10 and aGAR1 (CNG, 200 mM each) for 80 min at 65°C. Treatment with CMCT was carried out for 2, 10 or 20 min as described in Materials and Methods section with (+) or without (−) alkaline treatment. Positions of Ψ residues were identified by primer extension analysis using oligonucleotide OG 4891 (represented by the arrow in panel A1). Lanes U, G, C and A correspond to the RNA sequencing ladder. (**A4**) Time course of Ψ55 formation by aCBF5 protein in the *P. abyssi* tRNA^{Asp} and effect of the addition of proteins aNOP10 and aGAR1. The *P. abyssi* tRNA^{Asp} substrate was labeled as in panel A2 and incubated with various protein combinations: aCBF5 alone (C), aCBF5 and aNOP10 (CN), aCBF5 and aGAR1 (CG), a set of the three proteins (CNG) or TruB. For each time point, an aliquot of the reaction mixture was analyzed by 2D TLC. The amount of Ψ residue was estimated as in panel A2. (**B1**) Secondary structure of the *S. cerevisiae* tRNA^{Asp}. The sequence of oligonucleotide OG 5302 used as the primer for reverse transcription is indicated by an arrow. (**B2**) 2D-TLC analysis of Ψ formation by aCBF5 in the *S. cerevisiae* tRNA^{Asp} (same conditions as in panel A2). (**B3**) Detection of Ψ55 formation in the yeast tRNA^{Asp} by the CMC/RT approach (same conditions as in panel A3).

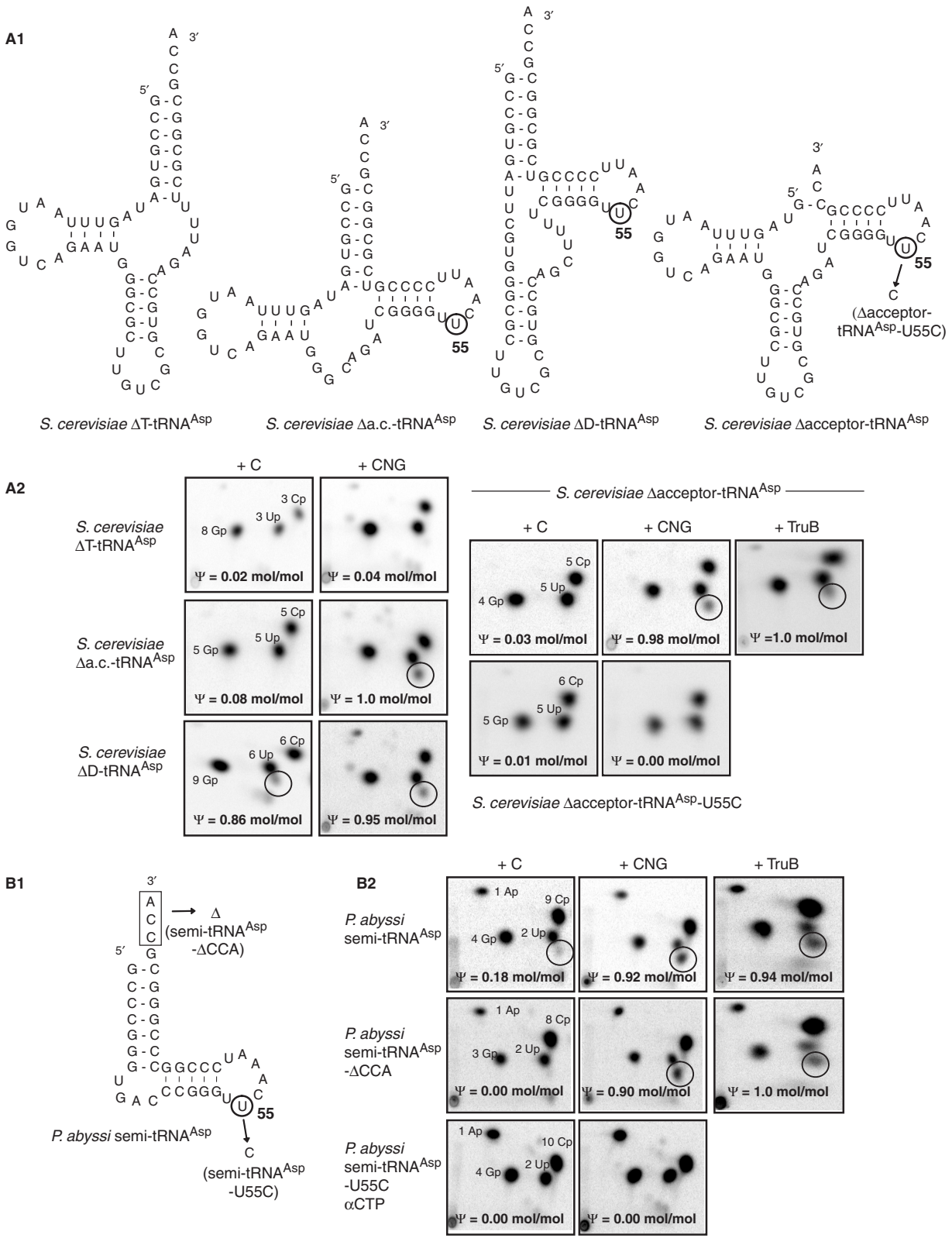

Figure 4. tRNA structural requirements for Ψ55 formation by aCBF5 or the aCBF5–aNOP10–aGAR1 complex. (**A1**) Secondary structure of the yeast truncated tRNAs^{Asp} used in this study. The DNA templates for transcription of the ΔT-tRNA^{Asp}, Δa.c.-tRNA^{Asp}, ΔD-tRNA^{Asp} and Δacceptor-tRNA^{Asp} were obtained by deletion of the T stem-loop, anticodon stem-loop, D stem-loop and acceptor stem sequences of the *S. cerevisiae* tRNA^{Asp} template sequence (Figure 1B1). (**B1**) The template sequence for the semi-tRNA^{Asp} was obtained by successive site-directed mutagenesis of the *P. abyssi* tRNA^{Asp} template sequence. (Figure 1A1). The variant semi-tRNA^{Asp}-ΔCCA with a deletion of the CCA sequence and the variant semi-tRNA^{Asp}-U55C with a U to C substitution are shown. (**A2** and **B2**) 2D-TLC analysis of Ψ formation by aCBF5, the aCBF5–aNOP10–aGAR1 complex or TruB, in the various truncated tRNAs. The same experiments conditions as in Figure 1A2 and B2 were used.

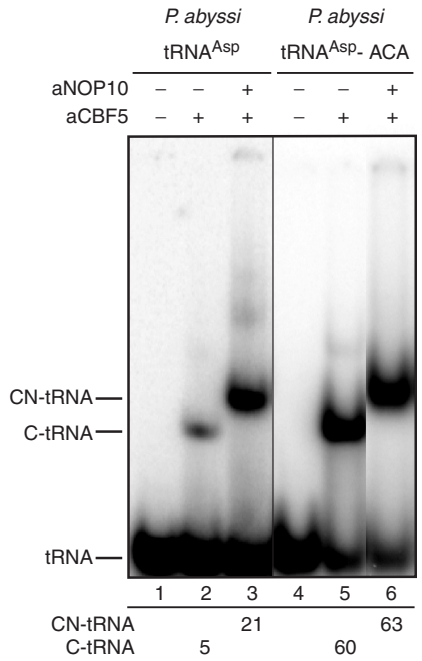

Figure 5. Analysis by electrophoresis mobility shift assays (EMSA) of the complexes formed between protein aCBF5 and archaeal tRNAs. The radiolabeled $tRNA^{Asp}$ (lanes 1–3) or $tRNA^{Asp}$-ACA (lanes 4–6) (50 fmol) were incubated with aCBF5 protein (C) (200 nM), in the presence or the absence of aNOP10 (N) (200 nM) as indicated on top of each lane. Positions of the various complexes C–tRNA and CN–tRNA are indicated on the left side of the autoradiogram. The amount of the complexes was estimated as described in Materials and Methods section.

this possibility, we estimated by EMSA experiments the level of complexes formed by the association of aCBF5 with a ^{32}P-labeled *P. abyssi* $tRNA^{Asp}$. The tests were performed in the presence or absence of aNOP10 (Figure 5). The level of complex formation was increased by a factor of ~4 in the presence of aNOP10 (Figure 5, compare lane 2 with lane 3), whereas no significant increase was observed in the presence of aGAR1 (data not shown). As aCBF5 is known to interact with the ACA conserved sequence of H/ACA sRNAs, we compared the affinity of aCBF5 for the WT $tRNA^{Asp}$ to that for a tRNA carrying an ACA triplet instead of the CCA triplet. The affinity of aCBF5 was indeed largely increased in the presence of an ACA triplet (Figure 5, compare lane 2 with lane 5) and aNOP10 did not increase the level of complex formation in this case (Figure 5, lane 6). Therefore, the stimulatory effect of aNOP10 on the kinetics of aCBF5 action on tRNAs may in part be due to its capability to facilitate the aCBF5–tRNA interaction. As previously observed for the aCBF5–RNA-guided activity, the stimulatory effect of aGAR1 on the aCBF5 activity is likely of another nature.

The conserved H31 and P32 residues in aNOP10 have different implications for the RNA-guided and non-RNA-guided activities of aCBF5

Based on the 3D structures established for the aCBF5–aNOP10 dimer and the aCBF5–aNOP10–aGAR1 trimer, the direct interactions between some conserved residues in the central flexible linker of aNOP10 (Figure 6A) with conserved residues of aCBF5 were proposed to influence the sRNA-guided activity of aCBF5 (28,29). In particular, the aNOP10 residues Y14 and H31 were found to form hydrogen bonds with residues E199 and R201 which are present in the β12 strand of aCBF5 (Figure 6B) (29). These interactions were proposed to influence the orientation of the side-chain of residue R202 that is located on the opposite face of the β12 strand. Interestingly, in the crystal structure of the complex formed between the *E. coli* TruB RNA:Ψ-synthase and a tRNA T stem-loop, the counterpart of residue R202 was proposed to interact with the phosphate on the 5′ side of the targeted uridine (31). On the other hand, in the aCBF5–aNOP10 complex, residue P32 in the aNOP10 flexible linker was found to interact by Van der Waals interaction with the conserved residue P54, which is located in motif I of aCBF5 (Figure 6C). This interaction was proposed to facilitate the formation of an hydrogen bond between residue K53 and the carbonyl oxygen of the catalytic residue D82 (28).

In light of these structural data, we used alanine substitutions to test for the relative importance of residues Y14, H31 and P32 for the RNA-guided and non-RNA-guided activities of aCBF5. Aiming at this, the stimulatory effects of each aNOP10 variant (Y14A, H31A and P32A) on the aCBF5 activity were tested on both the *P. abyssi* $tRNA^{Asp}$ lacking the CCA sequence (Figure 6D) and the RNA-S substrate (RNA target) of the *P. abyssi* Pab91 sRNPs (Figure 6F). To this end, sRNPs were reconstituted with each of the variant aNOP10 proteins. Whereas the H31A substitution had only a limited effect on the kinetics and the yield of Ψ55 formation in the archaeal $tRNA^{Asp}$ (Figure 6D), the Y14A substitution strongly slowed down the kinetics of this modification and the P32A substitution had a negative effect on the modification yield (~0.7 mol of Ψ per mole of tRNA, instead of ~0.9 mol of Ψ per mole of tRNA in the presence of the WT aNOP10 protein). Interestingly, the Y14A and P32A variants only had a limited effect on the sRNA-guided activity of aCBF5 (Figure 6F). The H31A mutation was in contrast strongly deleterious for this activity: only ~0.2 mol of Ψ per mole of target RNA was obtained after a 80 min incubation. Hence, mutations in aNOP10 have marked different effects on the RNA-guided and non-RNA-guided activities of aCBF5.

To try to define the reasons for the observed differences, we tested by EMSA the ability of the aNOP10 variant proteins to reinforce the aCBF5 association with the *P. abyssi* $tRNA^{Asp}$ and with the Pab91 sRNA and its target RNA sequence (Figure 6E and G). In agreement with the time-course results, both Y14A and P32A aNOP10 variants were less efficient (~0.5-fold) than the H31A aNOP10 variant and the WT aNOP10 protein for increasing the aCBF5 association with the tRNA (Figure 6E). On the contrary, only the H31A variant had a dramatic effect on the yield of complex CII (sRNA-L7Ae-aCBF5-aNOP10-RNA target) formation, suggesting that the H31A mutation has an important negative effect on substrate recruitment in the H/ACA sRNP. Therefore, we concluded that whereas residues

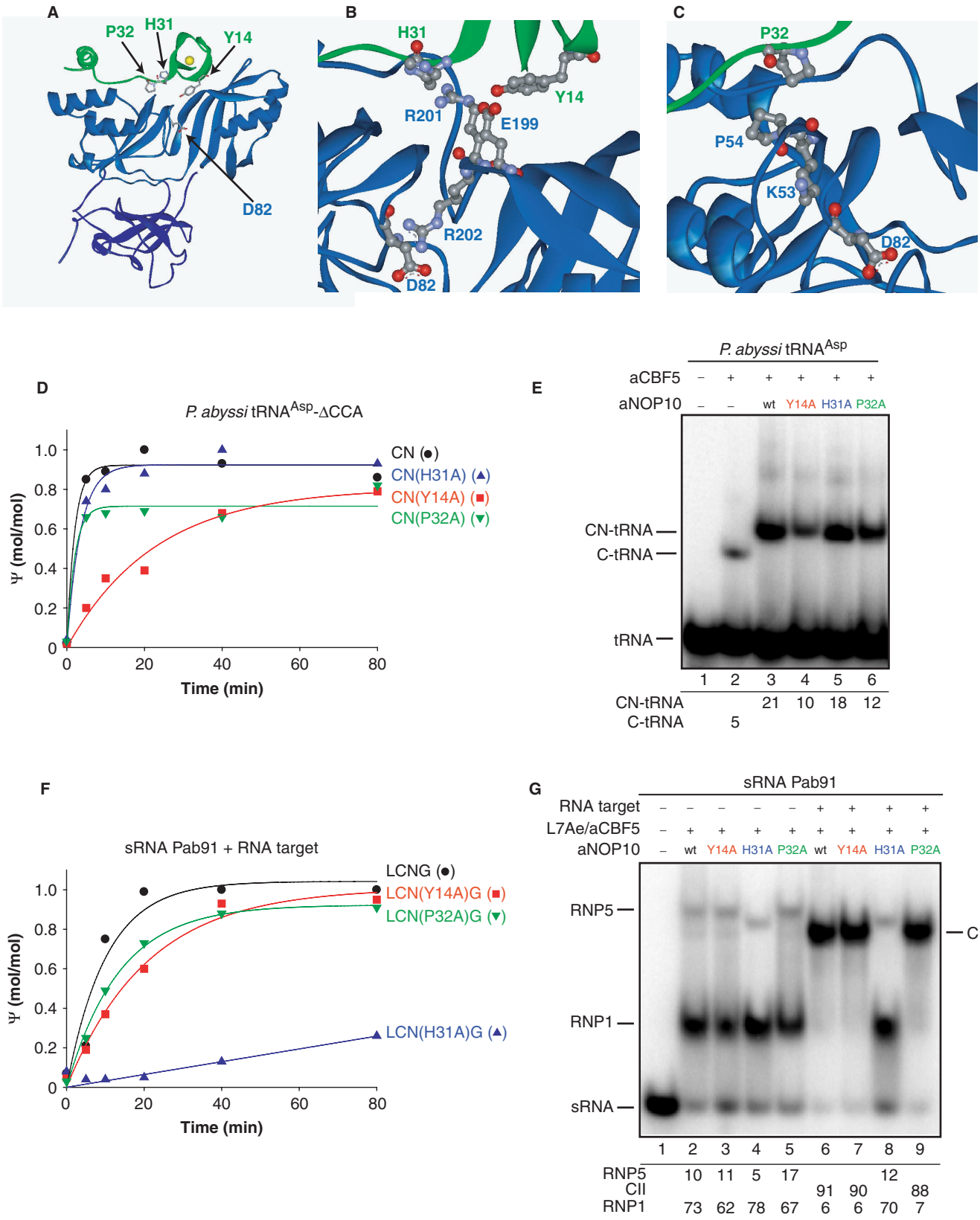

Figure 6. Role of the conserved residues in the aNOP10 protein for the non-RNA-guided and RNA-guided activities of aCBF5. (**A**) Ribbon representation of the heterodimer formed by interaction of aCBF5 (blue) with aNOP10 protein (green). The side chains of the aNOP10 residues P32, H31 and Y14 are represented, as well as the aCBF5 catalytic D82. (**B**) The residues expected to be involved in a network of interactions between aNOP10 and aCBF5 (29) are indicated on the *P. abyssi* structure. (**C**) Residues proposed to be involved in another network of interaction between aNOP10 and aCBF5 (28) are shown on the *P. abyssi* structure. (**D**) Time course of Ψ55 formation by aCBF5 (C) in the presence of the wild-type (N)

Y14 and P32 are highly important for the aCBF5 tRNA:Ψ55-synthase activity, residue H31 plays an essential role in substrate recruitment in the sRNA-guided activity of aCBF5.

aNOP10 and aGAR1 can compensate for R202A and K53A mutations in aCBF5 for the non-guided but not for the RNA-guided activity

Next, we tested the role of the aCBF5 residues R202 and K53 whose functions in the catalytic activity were proposed to be modulated by the aNOP10 residues H31 and Y14, and by residue P32, respectively (28,29). The aCBF5 variants R202A and K53A were produced, and the effect of each substitution was tested on both RNA-guided and non-RNA-guided activities. As evidenced in Figure 7A1, both R202A and K53A substitutions in aCBF5 abolished its activity at position 55 in the *P. abyssi* $tRNA^{Asp}$. However, this activity was fully restored upon addition of aNOP10 and aGAR1 in the incubation mixture (Figure 7A3). Here again, as evidenced by EMSA, the defect of activity observed for CBF5 alone was at least in part due to its low affinity for the tRNA (Figure 7A2). The addition of aNOP10 enhanced the association of aCBF5 with the tRNA, which likely explains the restoration of the tRNA:Ψ55-synthase activity. Hence, residues R202 and K53 likely play a role in tRNA association and aNOP10 can compensate for their mutations. In contrast, aNOP10 and aGAR1 were not able to compensate the negative effect of the R202A and K53A mutations in aCBF5 for the Pab91 sRNP activity (Figure 7B1), and here again, the low activity of the reconstituted sRNPs could be explained by a defect in substrate recruitment as the CII complex was formed at lower yields and displays a peculiar electrophoretic mobility (Figure 7B2, lanes 7 and 9). Hence, we concluded that residues K53 and R202 are important for tRNA binding in the non-RNA-guided system and for recruitment of the RNA substrate in the RNA-guided system. However, in this latter case, aNOP10 and aGAR1 cannot compensate for the absence of these residues. Therefore, residues R202 and K53 appear to play a more crucial role in the RNA-guided than in the non-RNA-guided system.

For both the RNA-guided and non-RNA-guided activities, the aCBF5 conserved residue H77 is dispensable in the presence of aNOP10 and aGAR1

In the *E. coli* TruB enzyme, residue H43 was proposed to be involved in the flipping of residue U55 out of the helical stack (31). The counterpart of residue H43 in aCBF5 is residue H77. As expected, the H77A mutation in aCBF5 almost completely impaired the aCBF5 activity on tRNA (Figure 7A1) and this is also likely to be explained by the lower affinity of aCBF5 for the tRNA (Figure 7A2). However, this activity could be restored in the presence of aNOP10 and aGAR1 (Figure 7A3) and we showed that protein aNOP10 restored an efficient association of aCBF5 with the tRNA (Figure 7A2). Interestingly, the H77A mutation had a very limited effect on the Pab91 sRNP activity (Figure 7B1) consistent with an efficient recruitment of the RNA substrate observed for this variant (Figure 7B2). Hence, we concluded that residue H77 does not play an essential role for the aCBF5 RNA:Ψ-synthase activity, provided that the aNOP10 and aGAR1 proteins are present.

DISCUSSION

The present data shed light on common and specific properties of aCBF5 and TruB. They also bring a comparative analysis of the sRNA-guided and non-guided activities of aCBF5. Finally, they delineate the role of aNOP10 in the aCBF5 non-guided activity.

The major role of the PUA domain in tRNA recognition by aCBF5

Interestingly, we found that aCBF5 does not modify the Δa.c.-$tRNA^{Asp}$ and Δacceptor-$tRNA^{Asp}$ but can act on the ΔD-$tRNA^{Asp}$. Therefore, like for TruB, the 3D structure of tRNA is not required for recognition of the targeted U residue in tRNAs by aCBF5. However, in addition to the T stem-loop, both the anticodon stem-loop and acceptor stem contain determinants which are necessary for aCBF5 activity on tRNAs. By these extended structural requirements, aCBF5 differs from TruB, that is able to use the T stem-loop alone as a substrate (46). This different behavior may be due to variations in both the catalytic and PUA domains of aCBF5 compared to the ones of TruB. The importance of the PUA domain for the aCBF5 tRNA:Ψ55-synthase activity is demonstrated by abolition of this activity upon PUA truncation. Previous data also revealed the strong importance of the PUA domain for H/ACA sRNP activity (27). Consistently, in the H/ACA sRNP structure, numerous protein contacts take place with the minor groove of the P1 stem and the conserved ACA motif (30). Although no 3D structure was established for an H/ACA sRNP bound to its substrate, recent NMR data (47,48) suggest that the heterologous helix P1S, which is formed by interaction of the 3′ strand of the pseudouridylation pocket and the target RNA, is coaxially stacked on helix P1 of the sRNA and altogether these two helices contain a rather conserved number of base pairs (10–12).

or variants H31A (filled triangle), Y14A (filled square), P32A (filled inverted triangle) of aNOP10 protein in the tRNA-ΔCCA. Experiments were performed as in Figure 1A4. (**E**) Analysis by EMSA of the complexes formed with the radiolabeled $tRNA^{Asp}$, the aCBF5 protein with or without the WT or variant Y14A, H31A and P32A aNOP10 proteins. (**F**) Time-course analysis of the RNA-guided Ψ formation in an RNA target. The previously described Pab91 sRNA target (36) was radiolabeled during transcription by incorporation of [α-^{32}P]CTP. It was incubated at 65°C with the unlabeled *P. abyssi* Pab91 sRNA, and the three *P. abyssi* proteins L7Ae (L), aCBF5 (C) and aGAR1 (G) with the WT (N) (filled circle) or variant aNOP10 proteins (indicated as in panel D). After T2 RNase digestion, the amount of Ψ formation was estimated by 1D-TLC analysis. (**G**) Analysis by EMSA of the amount of the RNP5 and CII complexes (36), formed with the radio-labeled Pab91 sRNA (50 fmol), proteins L7Ae, aCBF5 and either the WT or variants aNOP10. The formation of complex CII was obtained by incubation of the guide sRNA with the protein mixture and a 50 molar excess of an unlabeled RNA target, which carries a *P. abyssi* 23S rRNA fragment complementary to the Pab91 pseudouridylation pocket.

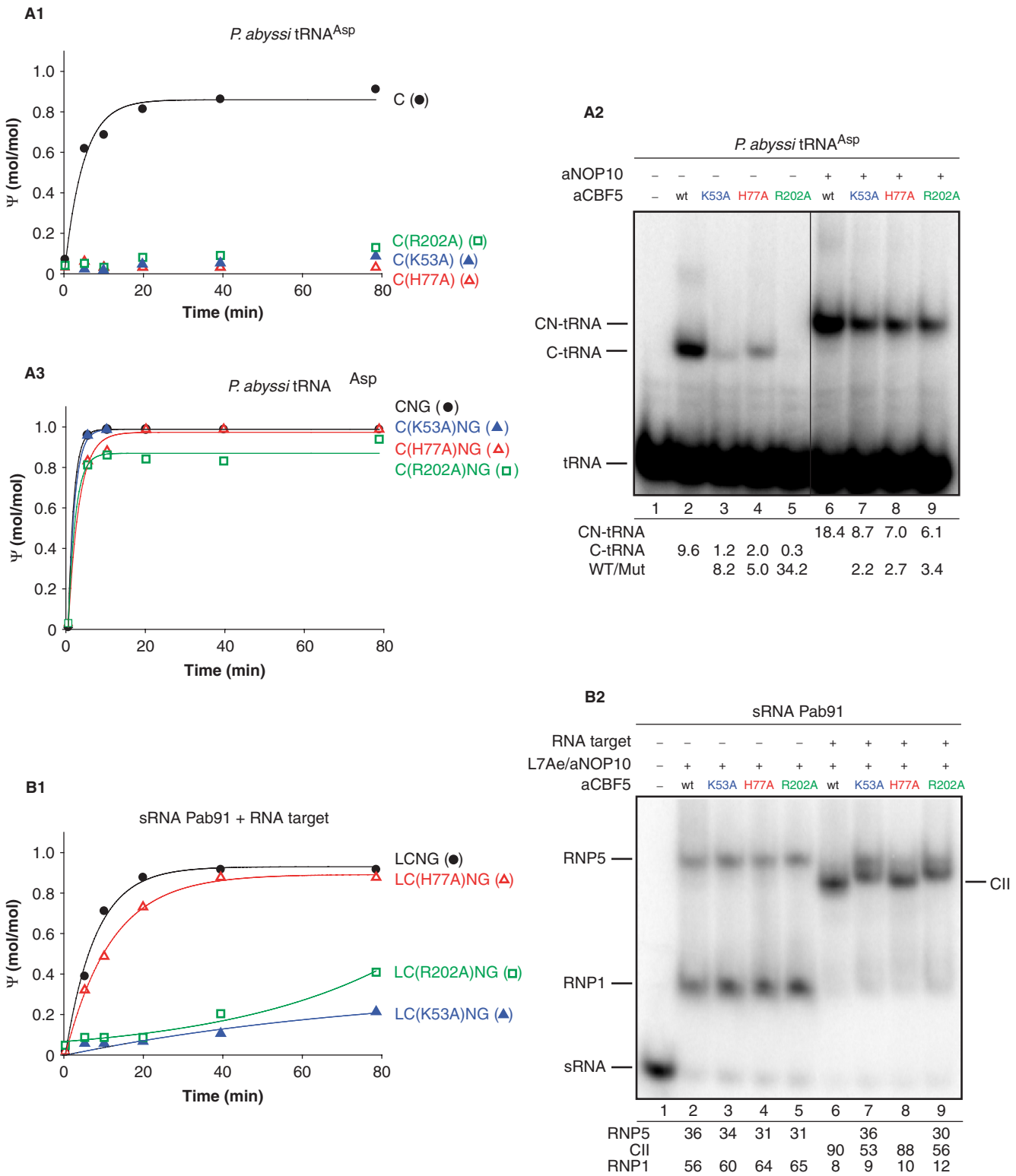

Figure 7. Effect of the substitution of residues in the aCBF5 catalytic site on its non-RNA-guided and RNA-guided activities. (**A1**) Time-course analysis of the non-RNA-guided Ψ55 formation in $tRNA^{Asp}$ by the wild type (C) (filled circle), or K53A, H77A and R202A variant aCBF5 proteins (filled triangle, open triangle, open square, respectively). Analysis was performed as in figure 1. (**A2**) Analysis by EMSA of the complexes formed with the radiolabeled $tRNA^{Asp}$, the WT (C) or variant aCBF5 proteins in the presence or absence of aNOP10 (N). The percentages of bound tRNA in the presence of WT or mutated aCBF5 and in the absence (C–tRNA) or presence of aNOP10 (CN–tRNA) are given as well as the ratios between tRNA bound to the mutated aCBF5 proteins versus that bound to WT aCBF5. (**A3**) The same experiments as in panel A1 were performed but in the presence of the auxiliary proteins aNOP10 (N) and aGAR1 (G). (**B1**) Time-course analysis of an RNA-guided Ψ formation carried out as in Figure 6F with the wild type or variant K53A, H77A and R202A aCBF5 proteins. (**B2**) Analysis by EMSA of the RNP5 and CII complexes. The experiments were performed as in Figure 6G, except that the variant aCBF5 proteins are used.

The heterologous helix P2S, that is formed with the 5′ strand of the pseudouridylation pocket, is basically stacked with the upperstem of the sRNA (P2) (47,48). The similarity between the T stem-loop structure recognized by TruB and the P2S heterologous helix formed by the guide RNA and the RNA substrate was pointed out (30,31). The tRNA acceptor stem flanked by the CCA motif would correspond to helix P1 of the sRNA and its conserved ACA motif, respectively. Based on this assumption, the finding that helix P1S, but not P2S, is stacked on the P1 stem of the sRNA can explain the requirement of a flexible link between the T and acceptor stem for aCBF5 activity. On the basis of this model of interaction between aCBF5 and tRNAs, the CCA motif of the tRNA, referred to the PUA domain, likely has the same position as the conserved ACA motif of H/ACA sRNAs (30). Therefore, like in TruB, the PUA domain of aCBF5 may interact with both the T and acceptor stems and the CCA motif, which explains the requirement of the acceptor stem and the 3′ terminal CCA for activity of the free aCBF5 protein (Figures 3 and 4). It should be pointed out that although TruB is active on the T stem-loop alone, the solved 3D structures of the RNA free and RNA bound TruB revealed, that upon tRNA binding, the PUA domain in TruB moves towards the active site and also makes interactions with residues of the acceptor stem (25). In the H/ACA sRNP structure, the two conserved adenosines of the ACA motif developed both stacking interactions and hydrogen bounds with several residues of the aCBF5 PUA domain. In particular, the 5′ proximal A residue inserts into an RNA-protein hybrid pocket formed between ribose moieties of the RNA minor groove and protein residues (30). Pocket formation is induced by RNA binding. Our gel-shift assays demonstrate a lower affinity of aCBF5 for a tRNA with an authentic CCA 3′ terminal sequence compared to a mutated tRNA with an ACA 3′ terminal sequence. Hence, an important issue would be to know how the RNA–protein interaction takes place when the proximal A residue in ACA is replaced by a C residue. The lower affinity for a CCA sequence compared to an ACA sequence may explain the needed interaction with the anticodon stem-loop for full activity of the free aCBF5 enzyme. This interaction may mimic that of aCBF5 with helix P2 in the sRNP. Interestingly, ACA to CCA substitution in a sRNA decreased substantially the amounts of aCBF5–sRNA complexes (data not shown). As aCBF5 is expected to have evolved from a pre-existing free standing enzyme, it would be interesting to investigate by 3D structure analysis of an aCBF5–tRNA complex, how the PUA domain of the pre-existing enzyme evolved in order to recognize both tRNAs and sRNAs.

It should also be pointed out that another possible explanation for the absence of activity on tRNAs of an aCBF5 without PUA domain may be the low thermostability of the truncated protein. Indeed, in contrast to the full-length aCBF5, the truncated aCBF5 cannot be enriched in the *E. coli* cellular extract by heating at 65°C. It precipitated with the *E. coli* proteins. Therefore, the PUA domain of aCBF5, which is wrapped by the N-terminal extremity of the molecule, likely plays an important role for aCBF5 thermostability.

Proteins aNOP10 and aGAR1 but not L7Ae reinforce the activity of aCBF5 on tRNAs

Whereas the individual addition of aNOP10 or aGAR1 stimulates the kinetics of aCBF5 activity on tRNA (Figure 1), no stimulatory effect was detected in the presence of L7Ae (Figure S1). A reasonable explanation is the absence of stable interaction between aCBF5 and L7Ae, while both aNOP10 and aGAR1 directly interact with this protein, as well in the presence, as in the absence of sRNA (35,36). Indeed, a direct interaction is formed between aNOP10 and L7Ae in the H/ACA sRNP structure (30), but this interaction is not stable by itself, it depends upon the binding of L7Ae on the K-turn or K-loop structure of the H/ACA sRNA. Based on these observations, it is reasonable to propose that aCBF5 can either act alone on tRNAs or in association with aNOP10 and aGAR1 *in vivo*. *In vitro*, the stimulatory effects of both aNOP10 and aGAR1 are particularly strong for tRNAs lacking the CCA sequence (Figure 3) and each of these proteins can compensate for the absence of this sequence. Therefore, it might be that in archaeal cells, the aCBF5-aNOP10, aCBF5-aGAR1 or aCBF5–aNOP10–aGAR1 complexes would modify archaeal tRNA precursors, before activity of the CCA-terminal transferase (49).

Our gel-shift assays strongly suggest that the activation property of aNOP10 on aCBF5 results in part from its capability to increase tRNA binding to aCBF5. In the 3D structure of an H/ACA sRNP, aNOP10 only forms a few contacts with the guide sRNA (30). However, aNOP10 is required for an efficient association of the substrate RNA on the complex formed by the guide sRNA and aCBF5 (36). Similarly, the tight interaction that aNOP10 established with aCBF5 (27–30) probably favors the tRNA recruitment (Figure 5). This aNOP10 activity together with the peculiarity of the aCBF5 PUA domain may compensate for the absence of the Ins1 and Ins2 segments in the aCBF5 catalytic domain as compared to the TruB catalytic domain. The Ins1 and Ins2 segments play a crucial role for TruB activity, since Ins2 forms the floor of the TΨC loop binding cavity and the Ins1 a binding thumb clamping this loop in the cavity (31). The disappearance of these two segments in aCBF5 is likely required to accommodate in the active site the sRNP four-helix-bundle structure formed upon annealing of a target RNA to the sRNA pseudouridylation pocket. The lack of Ins1 and Ins2 segments in aCBF5 may explain the strong requirement for the CCA 3′'-terminal motif, the acceptor stem and anticodon stem-loop for full activity of the free aCBF5 protein on tRNAs. It also likely explains the enhancer effect on activity of aNOP10, which increases the tRNA affinity. Up to now, the role of aGAR1 in the sRNA-guided system is less understood. GAR1 interacts with the RNA substrate in eukaryal snoRNP (50). However, this interaction seems to depend upon an additional domain present in the eukaryal protein as

compared to the archaeal protein. The protein aGAR1 also develops strong contact with the aCBF5 catalytic domain (29,30). Nonetheless, this may not help to reinforce the capability of aCBF5 to bind tRNA. In addition, aGAR1 was proposed to increase the turnover of the H/ACA sRNP (36). Therefore, this activity may also be needed to reinforce the aCBF5 tRNA:Ψ55-synthase activity.

Different networks of interaction are involved in the guided and non-guided activities of aCBF5

As mentioned above, the limited number of contacts between aNOP10 and the RNA in the H/ACA sRNP (30) suggests that the observed reinforcement of tRNA association in the presence of aNOP10 largely results from subtle conformational changes in the aCBF5 catalytic domain upon aNOP10–aCBF5 interaction. Superimposition of the 3D structures of the free and RNA-bound TruB enzyme (51) with the 3D structure of aCBF5 within the aCBF5–aNOP10 heterodimer shows a comparable positioning of the catalytic residues (27–30). In the absence of 3D structure of the free aCBF5 protein, we assume that in the free aCBF5 enzyme, an induced fit process has to take place upon tRNA binding for the optimization of the active site conformation. Interestingly, our data show that distinct residues of aNOP10 are involved in activation of the RNA-guided and non-guided activities of aCBF5 (Figure 6). Two conserved residues Y14 and H31 of aNOP10 were proposed to act in a common network of interactions linking aNOP10 to residue R202 in the aCBF5 catalytic site (29). Our data strongly suggest that the correct positioning of residue R202 in aCBF5 within the H/ACA sRNP involves residue H31 but not residue Y14, whereas the correct positioning of residue R202 for efficient tRNA:Ψ55-synthase activity depends upon residue Y14. Hence, conservation of these two residues in the course of evolution may reflect the conservation of the two enzymatic activities of aCBF5. Our data demonstrate a functional role in both the tRNA:Ψ55-synthase activity and the sRNA-guided activities of the conserved K residue in the aCBF5 motif I (K53 in aCBF5 and its counterpart K19 in *E. coli* TruB) (Figure 7). This residue is involved in the binding of the tRNA substrate and in the recruitment of the target RNA of the sRNP. Our data also show that the conserved P32 residue in aNOP10, which was proposed to link aNOP10 to the aCBF5 motif I (28), is essential, neither for the tRNA:Ψ55-synthase activity nor for the sRNA-guided activity. Another illustration of the difference between the aCBF5 RNA-guided and non-guided activities is the capability of aNOP10 to compensate for the absence of the lateral chains of residues K53 and R202 in the aCBF5 tRNA:Ψ55-synthase activity, but not in the sRNA-guided aCBF5 activity (Figure 7A3 and B1). Similarly, the substitution of residue K19 only has a mild effect on the TruB activity and leads to a thermosensitivity of the enzyme (52). Interestingly, the mutation of the conserved proline in motif I in the yeast Cbf5p also leads to a thermosensitivity of this enzyme (52,53). In light of these data, the positive effect of aNOP10 on the K53A aCBF5 variant may consist in a structural stabilization of motif I in the aCBF5–aNOP10 complex, allowing the reaction to proceed at the 65°C incubation temperature.

Residue R202 is specifically conserved in members of the TruB family. Its lateral chain is expected to interact with the 5′ phosphate of the targeted U residue (31). In agreement with these findings, we found that the R202A substitution affects tRNA association with aCBF5 and the binding of the target RNA on H/ACA sRNPs (Figure 7). Here again, protein aNOP10 can compensate for the R202A substitution. Another residue in the TruB catalytic center (Y76 from motif II) is expected to interact with the targeted U residue and is proposed to act as a general base during the catalytic mechanism (54). Other residues in aCBF5, like Y76 and/or Y179 which are expected to be located in the vicinity of the targeted U residue, can participate to the stabilization of the targeted residue. Interaction of aNOP10 with aCBF5 may favor their activity by subtle conformational changes in the aCBF5 active site.

Conservation of the crucial flipping mechanism in aCBF5

Upon tRNA binding on TruB, the uracil base at position 55 in the TΨC loop is extruded from the tRNA structure by a base-flipping mechanism that opens the tRNA 3D structure. Residue H43 probably plays a crucial role in this activity (31). Our observation that the mutation of residue H77, the counterpart of H43 in aCBF5, abolishes its tRNA:Ψ55-synthase activity strongly suggests that a similar mechanism is used for tRNA modification by aCBF5. Interestingly, aNOP10 can compensate for the H77A substitution. It would be highly interesting to determine by structural analysis how residue U55 is flipped out in the aCBF5 H77A variant associated with aNOP10. We also found that the RNA-guided activity is not impaired by the H77A substitution and this may be due to the fact that extrusion of the targeted U residue in H/ACA sRNPs is mainly mediated by the interaction between the guide and the target RNAs (47,48).

In spite of the absence of requirement of residue H77 for H/ACA sRNP activities, it should be noted that this residue is present in the eukaryal orthologs of aCBF5. This raises the question of a possible activity of the eukaryal Cbf5p/Dyskerin enzyme at position 55 in some eukaryal tRNAs. In connection with this observation, it should be pointed out that Cbf5 was found to co-purify with the selenocysteine tRNA in the protist *Euglena gracilis* (55).

SUPPLEMENTARY DATA

Supplementary Data are available at NAR Online.

ACKNOWLEDGEMENTS

I. Motorin is thanked for helpful discussion. S.M. and J.–B.F. are fellows from the French Ministère de la Recherche et des Nouvelles Technologies (MNRT).

The work was supported by the Centre National de la Recherche Scientifique (CNRS), the MNRT and the PRST « Bioingénierie » of Région Lorraine. Funding to pay the Open Access publication charges for this article was provided by CNRS.

Conflict of interest statement. None declared.

REFERENCES

1. Rozenski,J., Crain,P.F. and McCloskey,J.A. (1999) The RNA Modification Database: 1999 update. *Nucleic Acids Res.*, **27**, 196–197.
2. Decatur,W.A. and Fournier,M.J. (2002) rRNA modifications and ribosome function. *Trends Biochem. Sci.*, **27**, 344–351.
3. King,T.H., Liu,B., McCully,R.R. and Fournier,M.J. (2003) Ribosome structure and activity are altered in cells lacking snoRNPs that form pseudouridines in the peptidyl transferase center. *Mol. Cell*, **11**, 425–435.
4. Sumita,M., Desaulniers,J.P., Chang,Y.C., Chui,H.M., Clos,L. II and Chow,C.S. (2005) Effects of nucleotide substitution and modification on the stability and structure of helix 69 from 28S rRNA. *RNA*, **11**, 1420–1429.
5. Badis,G., Fromont-Racine,M. and Jacquier,A. (2003) A snoRNA that guides the two most conserved pseudouridine modifications within rRNA confers a growth advantage in yeast. *RNA*, **9**, 771–779.
6. Meroueh,M., Grohar,P.J., Qiu,J., SantaLucia,J.Jr, Scaringe,S.A. and Chow,C.S. (2000) Unique structural and stabilizing roles for the individual pseudouridine residues in the 1920 region of *Escherichia coli* 23S rRNA. *Nucleic Acids Res.*, **28**, 2075–2083.
7. Kirpekar,F., Hansen,L.H., Rasmussen,A., Poehlsgaard,J. and Vester,B. (2005) The archaeon *Haloarcula marismortui* has few modifications in the central parts of its 23S ribosomal RNA. *J. Mol. Biol.*, **348**, 563–573.
8. Del Campo,M., Recinos,C., Yanez,G., Pomerantz,S.C., Guymon,R., Crain,P.F., McCloskey,J.A. and Ofengand,J. (2005) Number, position, and significance of the pseudouridines in the large subunit ribosomal RNA of Haloarcula marismortui and *Deinococcus radiodurans*. *RNA*, **11**, 210–219.
9. Yu,Y.T., Shu,M.D. and Steitz,J.A. (1998) Modifications of U2 snRNA are required for snRNP assembly and pre-mRNA splicing. *EMBO J.*, **17**, 5783–5795.
10. Yang,C., McPheeters,D.S. and Yu,Y.T. (2005) Psi35 in the branch site recognition region of U2 small nuclear RNA is important for pre-mRNA splicing in *Saccharomyces cerevisiae*. *J. Biol. Chem.*, **280**, 6655–6662.
11. Hamma,T. and Ferre-D'Amare,A.R. (2006) Pseudouridine synthases. *Chem. Biol.*, **13**, 1125–1135.
12. Kammen,H.O., Marvel,C.C., Hardy,L. and Penhoet,E.E. (1988) Purification, structure, and properties of *Escherichia coli* tRNA pseudouridine synthase I. *J. Biol. Chem.*, **263**, 2255–2263.
13. Nurse,K., Wrzesinski,J., Bakin,A., Lane,B.G. and Ofengand,J. (1995) Purification, cloning, and properties of the tRNA Psi 55 synthase from *Escherichia coli*. *RNA*, **1**, 102–112.
14. Wrzesinski,J., Bakin,A., Nurse,K., Lane,B.G. and Ofengand,J. (1995) Purification, cloning, and properties of the 16S RNA pseudouridine 516 synthase from *Escherichia coli*. *Biochemistry*, **34**, 8904–8913.
15. Wrzesinski,J., Nurse,K., Bakin,A., Lane,B.G. and Ofengand,J. (1995) A dual-specificity pseudouridine synthase: An *Escherichia coli* synthase purified and cloned on the basis of its specificity for Ψ746 in 23S RNA is also specific for Ψ32 in $tRNA^{phe}$. *RNA*, **1**, 437–448.
16. Koonin,E.V. (1996) Pseudouridine synthases: four families of enzymes containing a putative uridine-binding motif also conserved in dUTPases and dCTP deaminases. *Nucleic Acids Res.*, **24**, 2411–2415.
17. Kaya,Y. and Ofengand,J. (2003) A novel unanticipated type of pseudouridine synthase with homologs in bacteria, archaea, and eukarya. *RNA*, **9**, 711–721.
18. Behm-Ansmant,I., Urban,A., Ma,X., Yu,Y.-T., Motorin,Y. and Branlant,C. (2003) The *Saccharomyces cerevisiae* U2 snRNA:pseudouridine-synthase Pus7p is a novel multisite-multisubstrate RNA:Psi-synthase also acting on tRNAs. *RNA*, **9**, 1371–1382.
19. del Campo,M., Ofengand,J. and Malhotra,A. (2004) Crystal structure of the catalytic domain of RluD, the only rRNA pseudouridine synthase required for normal growth of *Escherichia coli*. *RNA*, **10**, 231–239.
20. Kaya,Y., Del Campo,M., Ofengand,J. and Malhotra,A. (2004) Crystal structure of TruD, a novel pseudouridine synthase with a new protein fold. *J. Biol. Chem.*, **279**, 18107–18110.
21. Huang,L., Pookanjanatavip,M., Gu,X. and Santi,D.V. (1998) A conserved aspartate of tRNA pseudouridine synthase is essential for activity and a probable nucleophilic catalist. *Biochemistry*, **37**, 344–351.
22. Ramamurthy,V., Swann,S.L., Paulson,J.L., Spedaliere,C.J. and Mueller,E.G. (1999) Critical aspartic acid residues in pseudouridine synthases. *J. Biol. Chem.*, **274**, 22225–22230.
23. Conrad,J., Niu,L., Rudd,K., Lane,B.G. and Ofengand,J. (1999) 16S ribosomal RNA pseudouridine synthase RsuA of *Escherichia coli*: deletion, mutation of the conserved Asp102 residue, and sequence comparison among all other pseudouridine synthases. *RNA*, **5**, 761–763.
24. Raychaudhuri,S., Niu,L., Conrad,J., Lane,B.G. and Ofengand,J. (1999) Functional effect of deletion and mutation of the *Escherichia coli* ribosomal RNA and tRNA pseudouridine synthase RluA. *J. Biol. Chem.*, **274**, 18880–18886.
25. Ferre-D'Amare,A.R. (2003) RNA-modifying enzymes. *Curr. Opin. Struct. Biol.*, **13**, 49–55.
26. Aravind,L. and Koonin,E.V. (1999) Novel predicted RNA-binding domains associated with the translation machinery. *J. Mol. Evol.*, **48**, 291–302.
27. Manival,X., Charron,C., Fourmann,J.B., Godard,F., Charpentier,B. and Branlant,C. (2006) Crystal structure determination and site-directed mutagenesis of the *Pyrococcus abyssi* aCBF5-aNOP10 complex reveal crucial roles of the C-terminal domains of both proteins in H/ACA sRNP activity. *Nucleic Acids Res.*, **34**, 826–839.
28. Hamma,T., Reichow,S.L., Varani,G. and Ferre-D'Amare,A.R. (2005) The Cbf5-Nop10 complex is a molecular bracket that organizes box H/ACA RNPs. *Nat. Struct. Mol. Biol.*, **12**, 1101–1107.
29. Rashid,R., Liang,B., Baker,D.L., Youssef,O.A., He,Y., Phipps,K., Terns,R.M., Terns,M.P. and Li,H. (2006) Crystal structure of a Cbf5-Nop10-Gar1 complex and implications in RNA-guided pseudouridylation and dyskeratosis congenita. *Mol. Cell*, **21**, 249–260.
30. Li,L. and Ye,K. (2006) Crystal structure of an H/ACA box ribonucleoprotein particle. *Nature*, **443**, 302–307.
31. Hoang,C. and Ferre-D'Amare,A.R. (2001) Cocrystal structure of a tRNA Psi55 pseudouridine synthase: nucleotide flipping by an RNA-modifying enzyme. *Cell*, **107**, 929–939.
32. Bachellerie,J.P., Cavaille,J. and Huttenhofer,A. (2002) The expanding snoRNA world. *Biochimie*, **84**, 775–790.
33. Kiss,T. (2002) Small nucleolar RNAs: an abundant group of noncoding RNAs with diverse cellular functions. *Cell*, **109**, 145–148.
34. Omer,A.D., Ziesche,S., Decatur,W.A., Fournier,M.J. and Dennis,P.P. (2003) RNA-modifying machines in archaea. *Mol. Microbiol.*, **48**, 617–629.
35. Baker,D.L., Youssef,O.A., Chastkofsky,M.I., Dy,D.A., Terns,R.M. and Terns,M.P. (2005) RNA-guided RNA modification: functional organization of the archaeal H/ACA RNP. *Genes Dev.*, **19**, 1238–1248.
36. Charpentier,B., Muller,S. and Branlant,C. (2005) Reconstitution of archaeal H/ACA small ribonucleoprotein complexes active in pseudouridylation. *Nucleic Acids Res.*, **33**, 3133–3144.
37. Khanna,M., Wu,H., Johansson,C., Caizergues-Ferrer,M. and Feigon,J. (2006) Structural study of the H/ACA snoRNP components Nop10p and the 3′ hairpin of U65 snoRNA. *RNA*, **12**, 40–52.
38. Rozhdestvensky,T.S., Tang,T.H., Tchirkova,I.V., Brosius,J., Bachellerie,J.P. and Huttenhofer,A. (2003) Binding of L7Ae protein to the K-turn of archaeal snoRNAs: a shared RNA binding motif

for C/D and H/ACA box snoRNAs in Archaea. *Nucleic Acids Res.*, **31**, 869–877.
39. Hamma,T. and Ferre-D'Amare,A.R. (2004) Structure of protein L7Ae bound to a K-turn derived from an archaeal box H/ACA sRNA at 1.8 A resolution. *Structure*, **12**, 893–903.
40. Roovers,M., Hale,C., Tricot,C., Terns,M.P., Terns,R.M., Grosjean,H. and Droogmans,L. (2006) Formation of the conserved pseudouridine at position 55 in archaeal tRNA. *Nucleic Acids Res.*, **34**, 4293–4301.
41. Charpentier,B., Fourmann,J.B. and Branlant,C. (2007) Reconstitution of archaeal H/ACA sRNPs and test of their activity. *Methods Enzymol.*, **425**, 389–405.
42. Bakin,A. and Ofengand,J. (1993) Four newly located pseudouridylate residues in *Escherichia coli* 23S ribosomal RNA are all at the peptidyltransferase center - analysis by the application of a new sequencing technique. *Biochemistry*, **32**, 9754–9762.
43. Massenet,S., Ansmant,I., Motorin,Y. and Branlant,C. (1999) The first determination of pseudouridine residues in 23S ribosomal RNA from hyperthermophilic Archaea *Sulfolobus acidocaldarius*. *FEBS Lett.*, **462**, 94–100.
44. Mougin,A., Gregoire,A., Banroques,J., Segault,V., Fournier,R., Brule,F., Chevrier-Miller,M. and Branlant,C. (1996) Secondary structure of the yeast *Saccharomyces cerevisiae* pre-U3A snoRNA and its implication for splicing efficiency. *RNA*, **2**, 1079–1093.
45. Motorin,Y., Muller,S., Behm-Ansmant,I. and Branlant,C. (2007) Identification of modified residues in RNAs by reverse transcription-based methods. *Methods Enzymol.*, **425**, 21–53.
46. Gu,X., Yu,M., Ivanetich,K.M. and Santi,D.V. (1998) Molecular recognition of tRNA by tRNA pseudouridine 55 synthase. *Biochemistry*, **37**, 339–343.
47. Jin,H., Loria,J.P. and Moore,P.B. (2007) Solution structure of an rRNA substrate bound to the pseudouridylation pocket of a box H/ACA snoRNA. *Mol. Cell*, **26**, 205–215.
48. Wu,H. and Feigon,J. (2007) H/ACA small nucleolar RNA pseudouridylation pockets bind substrate RNA to form three-way junctions that position the target U for modification. *Proc. Natl Acad. Sci. USA*, **104**, 6655–6660.
49. Tomita,K., Ishitani,R., Fukai,S. and Nureki,O. (2006) Complete crystallographic analysis of the dynamics of CCA sequence addition. *Nature*, **443**, 956–960.
50. Wang,C. and Meier,U.T. (2004) Architecture and assembly of mammalian H/ACA small nucleolar and telomerase ribonucleoproteins. *EMBO J.*, **23**, 1857–1867.
51. Pan,H., Agarwalla,S., Moustakas,D.T., Finer-Moore,J. and Stroud,R.M. (2003) Structure of tRNA pseudouridine synthase TruB and its RNA complex: RNA recognition through a combination of rigid docking and induced fit. *Proc. Natl Acad. Sci. USA*, **100**, 12648–12653.
52. Spedaliere,C.J., Hamilton,C.S. and Mueller,E.G. (2000) Functional importance of motif I of pseudouridine synthases: mutagenesis of aligned lysine and proline residues. *Biochemistry*, **39**, 9459–9465.
53. Zebarjadian,Y., King,T., Fournier,M.J., Clarke,L. and Carbon,J. (1999) Point mutations in yeast CBF5 can abolish in vivo pseudouridylation of rRNA. *Mol. Cell. Biol.*, **19**, 7461–7472.
54. Phannachet,K., Elias,Y. and Huang,R.H. (2005) Dissecting the roles of a strictly conserved tyrosine in substrate recognition and catalysis by pseudouridine 55 synthase. *Biochemistry*, **44**, 15488–15494.
55. Russell,A.G., Schnare,M.N. and Gray,M.W. (2004) Pseudouridine-guide RNAs and other Cbf5p-associated RNAs in *Euglena gracilis*. *RNA*, **10**, 1034–1046.